

Zero-Shot Medical Phrase Grounding with Off-the-shelf Diffusion Models

Konstantinos Vilouras , Pedro Sanchez , Alison Q. O’Neil , and Sotirios A. Tsaftaris , *Senior Member, IEEE*

Abstract—Localizing the exact pathological regions in a given medical scan is an important imaging problem that requires a large amount of bounding box ground truth annotations to be accurately solved. However, there exist alternative, potentially weaker, forms of supervision, such as accompanying free-text reports, which are readily available. The task of performing localization with textual guidance is commonly referred to as phrase grounding. In this work, we use a publicly available Foundation Model, namely the Latent Diffusion Model, to solve this challenging task. This choice is supported by the fact that the Latent Diffusion Model, despite being generative in nature, contains mechanisms (cross-attention) that implicitly align visual and textual features, thus leading to intermediate representations that are suitable for the task at hand. In addition, we aim to perform this task in a zero-shot manner, i.e., without any further training on target data, meaning that the model’s weights remain frozen. To this end, we devise strategies to select features and also refine them via post-processing without extra learnable parameters. We compare our proposed method with state-of-the-art approaches which explicitly enforce image-text alignment in a joint embedding space via contrastive learning. Results on a popular chest X-ray benchmark indicate that our method is competitive with SOTA on different types of pathology, and even outperforms them on average in terms of two metrics (mean IoU and AUC-ROC). Source code will be released upon acceptance.

Index Terms—Deep Learning, Diffusion Models, Medical Imaging, Phrase Grounding, Zero-shot learning

I. INTRODUCTION

THE rapid success of deep learning over the last few years has led to powerful data-driven models being deployed already in real-world scenarios. Recently, by taking advantage of the scaling properties of popular deep learning methods both

Manuscript submitted for review on 15 March 2024. This work was supported by the University of Edinburgh, the Royal Academy of Engineering and Canon Medical Research Europe by PhD studentships to Konstantinos Vilouras and Pedro Sanchez. S.A. Tsaftaris also acknowledges the support of Canon Medical and the Royal Academy of Engineering and the Research Chairs and Senior Research Fellowships scheme (grant RCSR1819\8\25), and the UK’s Engineering and Physical Sciences Research Council (EPSRC) support via grant EP/X017680/1.

Konstantinos Vilouras, Pedro Sanchez, Sotirios A. Tsaftaris are with the School of Engineering, University of Edinburgh, Edinburgh EH9 3FB, United Kingdom (e-mail: konstantinos.vilouras@ed.ac.uk, pedro.sanchez@ed.ac.uk, s.tsaftaris@ed.ac.uk).

Alison O’Neil is with Canon Medical Research Europe Ltd., Edinburgh EH6 5NP, United Kingdom (e-mail: alison.oneil@mre.medical.canon) and with the School of Engineering, University of Edinburgh, Edinburgh EH9 3FB, United Kingdom.

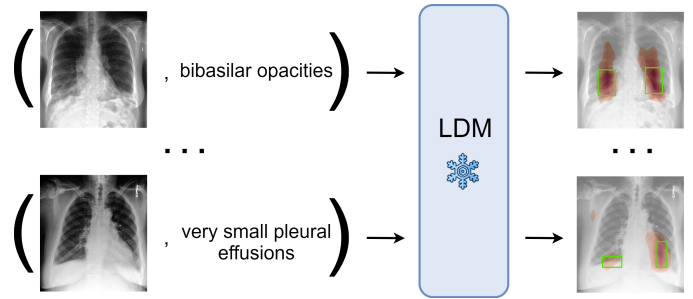


Fig. 1: High-level description of the zero-shot phrase grounding task. Given input pairs of an image (chest X-ray) and its accompanying text prompt, our goal is to leverage feature alignment mechanisms within a frozen Latent Diffusion Model (LDM) to extract heatmaps, which indicate the regions where image and text are maximally aligned. Then, we evaluate the generated heatmaps based on ground truth bounding boxes (shown in green) for pathology detection. Our method, thus, is an illustration of using pre-trained LDMs for downstream applications in a zero-shot setting.

in terms of learnable parameters and training data, we witness the era of Foundation Models (FMs) [1], i.e., large-scale neural networks that were trained on massive amounts of data. FMs have unprecedented capabilities: they can be readily applied to a wide variety of tasks as standalone solutions, or they can serve as a robust basis for training models on unknown tasks and, plausibly, modalities (e.g., transferring knowledge from natural images to the medical domain). Among their many benefits, FMs provide machine learning practitioners and researchers with a universal tool that enables the widespread application of data-driven solutions to multiple scientific fields, as well as the development of a sound theoretical framework around well-known deep learning methodologies.

In this work, we investigate a specific type of FM: the Latent Diffusion Model. We draw inspiration from research studies showing that diffusion models can solve downstream tasks such as classification [2], [3] and segmentation [4] with little to no additional fine-tuning on target data. Here, we attempt to validate this finding, that is the re-usability of diffusion models for downstream tasks, in the medical imaging domain, focusing on the *phrase grounding* task where the goal is to localize the pathology in an input scan (e.g., chest X-ray) given an accompanying textual description provided by expert clinicians. A high-level overview of our method for the phrase

grounding task is shown in Fig. 1.

We perform extensive experiments on an established phrase grounding benchmark dataset, i.e., MS-CXR [5]. The results suggest that, despite being inherently a generative model, the Latent Diffusion Model has learned high quality features for the task at hand. Our proposed approach, which tackles the extreme case where no additional fine-tuning is performed (we refer to it as a *zero-shot* scenario), yields, perhaps surprisingly, a highly competitive method that proves to be state-of-the-art in terms of two metrics (mean IoU and AUC-ROC) on average across 8 pathology labels.

Overall, our **contributions** can be summarized as follows:

- Building on the Latent Diffusion Model architecture, we propose a method to gather semantically meaningful visual features both from multiple timesteps of the reverse diffusion process and also from various cross-attention layers. We target those layers since they inherently align information from the visual and textual stream, thus being suitable for the phrase grounding task.
- We perform extensive experiments on a medical dataset with ground truth bounding boxes and test our method against several strong baselines. Results indicate that our method shows competitive performance against, and even exceeds in the case of two metrics, the current state-of-the-art without any fine-tuning strategies.
- We provide an ablation study to justify the different hyperparameter choices in our system.
- We further analyze qualitatively our proposed method, as well as the strongest available baseline, to provide useful insights for both approaches.

II. RELATED WORK

We now summarize the most relevant research. We start by mentioning prior influential works showing that diffusion models can be effectively applied to multiple downstream tasks in a zero- or few-shot setting. Then, we briefly discuss some of the most popular methods for phrase grounding in natural RGB images. Finally, we shift our focus to approaches related to the medical imaging domain, against which we compare our proposed method.

A. Downstream Application of Diffusion Models

Recent studies have revealed the ability of diffusion models to perform fairly well on downstream tasks. For example, for classification tasks it has been shown that the posterior $p(\mathbf{c}|\mathbf{x})$ for all candidate classes \mathbf{c} can be estimated from a diffusion model’s residual errors at a given timestep without any requirement for further hyperparameters or training [2], [3]. Similarly, for segmentation, Baranchuk *et al.* [4] use intermediate visual representations extracted from a diffusion model. In this case, a few additional labelled images are required to train a shallow network that outputs pixel-wise predictions. In another work, Zhao *et al.* [6] experiment with the text feature extraction pipeline, as well as the choice of intermediate visual features, and train lightweight task-specific models for segmentation and depth estimation, respectively.

B. Visual Phrase Grounding

Phrase grounding is a cross-modal reasoning task referring to the spatial localization of objects present in an image given a related text description. Due to the widespread availability of image-text data sources, there already exist large-scale end-to-end models for the natural image domain. In a discriminative learning scenario, ViLBERT [7] introduces the concept of co-attention, i.e., exchanging information between modalities within the transformer layers. Early fusion strategies are also adopted by MDETR [8] which enforces image-text alignment with appropriate learning objectives, and GLIP [9] in which image and language encoders are simultaneously trained to correctly assign a word to a specific image region. Chen and Li [10] follow a generative learning approach by training a text-guided diffusion model to gradually recover ground-truth bounding boxes from their noise-perturbed versions.

C. Medical Phrase Grounding

In the medical imaging domain, phrase grounding is considered a difficult task due to the inherent variation in textual information (radiologists, e.g., commonly use domain-specific terms, negations, or phrases that convey a level of uncertainty). Earlier works have taken different approaches. Bhalodia *et al.* [11] extract pneumonia-related attributes from radiology reports, while a pre-trained bounding box detector is used to extract regions of interest (ROIs) and their associated features. Then, using both streams of information, their system is trained to correctly classify attributes from visual features, as well as to maximize the similarity for a given image-text pair. End-to-end discriminative methods to date are largely fully supervised [12], [13] or rely on self-supervised contrastive formulations [5], [14], [15]. Specifically, Chen *et al.* [12] train a vision-language Transformer model to directly predict bounding boxes, whereas Xu *et al.* [13] gather publicly available labelled chest X-ray datasets and train a single model via multi-task learning. LIMITR [14] is a self-supervised method that aligns local cross-modal representations that are further weighted via learnable significance scores. Lastly, BioViL [5] is an end-to-end model with a BERT text encoder finetuned on radiology reports that is optimized via both global and local cross-modal contrastive losses. Bannur *et al.* [15] extend the BioViL model to support longitudinal information across patients, and the resulting system (BioViL-T) achieves state-of-the-art performance on medical phrase grounding.

In contrast, we adopt a generative approach to this task. A concurrent work also applies diffusion models to phrase grounding [16]. Our approach differs in several ways: First, we use a pre-trained, publicly available diffusion model and propose mechanisms to perform phrase grounding whilst keeping the model frozen, whereas [16] focuses on training the model from scratch. Second, to define these mechanisms, we pay attention to how we select cross-attention layers and timesteps, whereas [16] simply average across both time and layers. Finally, we compare our method with more recent state-of-the-art and other, recently proposed, baselines. Nevertheless, the findings of [16] are beneficial for our work. They show that learning both text and visual encoders simultaneously

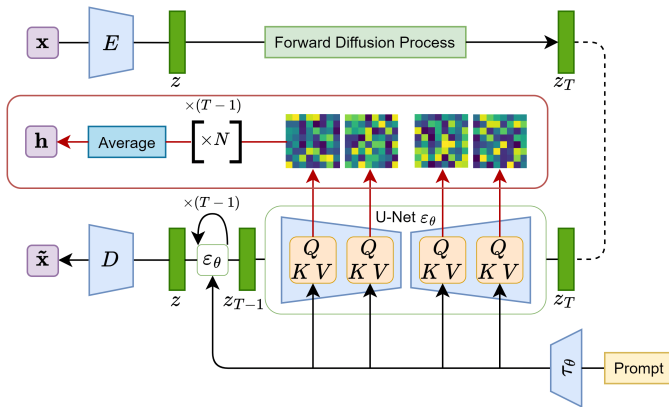


Fig. 2: Overview of our proposed phrase grounding pipeline based on the Latent Diffusion Model architecture [17]. The input image x is first passed through the encoder E . The resulting feature vector z is gradually mapped into an isotropic Gaussian after T time steps of the forward diffusion process. Then, a denoising U-Net ϵ_θ is tasked to sequentially transform noisy latents in reverse order, i.e., from step t to $t-1$, $t = 1, \dots, T$. To further aid this task, text embeddings (generated from the encoder τ_θ) are also introduced in the U-Net’s cross-attention blocks. We intervene on this setup by gathering the N attention maps from all cross-attention blocks within the U-Net ϵ_θ . Thus, by averaging a total of $N \cdot T$ attention maps, we end up with an activation heatmap \mathbf{h} for the given input.

severely degrades performance. In addition, regarding the textual information that is available for phrase grounding, they show that using sentences from the original radiology reports (as is the case, for example, for the MS-CXR [5] dataset) leads to the best overall results, outperforming both synthetically generated text (with ChatGPT) and the simplest case of using the class string as the input prompt.

III. METHODOLOGY

We adopt the following notation: x is a scalar, x denotes a vector, \mathbf{x} is a tensor, f_θ refers to the total number of a network’s f learnable parameters (weights), \mathcal{X} stands for a vector space, and $\mathbf{X} : \mathcal{X} \rightarrow \mathcal{X}$ is a neural network that performs a mapping between two vector spaces. We also consider a dataset $\mathcal{D} = \{\mathbf{x}_i, p_i\}_{i=1}^N$ with image-text pairs, where N is the total number of samples. For brevity, we will next discuss our pipeline while considering a single input (\mathbf{x}, p) ; the extension to a batch of samples is trivial.

A. Overview of the Latent Diffusion Model

The Latent Diffusion Model (LDM) [17] belongs to the class of probabilistic models and is considered one of the most groundbreaking methods for image synthesis. The versatile design of the LDM has significantly contributed towards its success, as external sources of information (e.g., text, segmentation masks, or any other type of a representation) can be easily incorporated into the model without any architectural changes. Here, we follow the standard setup of the LDM architecture as proposed in [17]. More specifically, via the

encoder $\mathbf{E} : \mathcal{X} \rightarrow \mathcal{Z}$, the input image \mathbf{x} is first encoded into a latent feature vector z which, in turn, is progressively corrupted with Gaussian noise via a deterministic forward diffusion process for a total of T timesteps. Then, for each timestep t , a denoising U-Net $\epsilon_\theta : \mathcal{Z} \rightarrow \mathcal{Z}$ is applied to the noisy latent z_t to recover the cleaner estimate at the previous step z_{t-1} . After the reverse diffusion process, the recovered global latent z is mapped to the original pixel space via a decoder $\mathbf{D} : \mathcal{Z} \rightarrow \mathcal{X}$, leading to the reconstructed input $\tilde{\mathbf{x}}$. An overview of the LDM pipeline is depicted in Fig. 2.

B. Image-Text Alignment via Cross-Attention

To aid reconstruction, textual information about the image \mathbf{x} is also injected in the U-Net model ϵ_θ in the form of a natural language prompt. Concretely, the prompt p that accompanies the input sample \mathbf{x} is projected into an embedding via a pre-trained text encoder τ_θ . The resulting text feature vector serves as context in each cross-attention block of the U-Net, i.e., it is used to generate keys \mathbf{k} and values \mathbf{v} for the self-attention operation as defined below, where \mathbf{q} refers to the queries extracted from the visual features, \mathbf{P}_K and \mathbf{P}_V are projection layers for the keys and values, respectively, and d is a scaling factor,

$$\mathbf{k} = \mathbf{P}_K(\tau_\theta(p)) \quad \mathbf{v} = \mathbf{P}_V(\tau_\theta(p))$$

$$\text{Attention}(\mathbf{q}, \mathbf{k}, \mathbf{v}) = \text{softmax}\left(\frac{\mathbf{q}\mathbf{k}^\top}{\sqrt{d}}\right) \cdot \mathbf{v}. \quad (1)$$

From Eq. (1), we observe that the LDM architecture contains a straightforward mechanism that aligns visual and textual features. Moreover, the model’s design provides access to information at different levels of granularity, since there are multiple cross-attention blocks in the U-Net, while the generated attention maps also vary across timesteps. Let N denote the total number of cross-attention blocks in the U-Net model and T the number of timesteps used for the diffusion process. That leaves us with $N \cdot T$ attention maps in total, where each one varies both on the content of the visual features (low-level features or higher-level semantics) or at the timestep of the reverse diffusion process, which directly affects the noise level of each latent z_t .

C. Zero-shot Phrase Grounding with the LDM

The trained LDM can be readily used to perform phrase grounding in a zero-shot setting. After gathering the $N \cdot T$ attention maps, we need to aggregate them to extract a single activation heatmap \mathbf{h} that matches the original input’s, \mathbf{x} , spatial dimensions (after appropriate up-scaling). In the ideal case of perfect image-text alignment, \mathbf{h} will be highly activated on the regions of interest specified by the prompt. In this paper, we simply average the gathered attention maps across layers and timesteps, experimenting with the selection of cross-attention blocks and timesteps to optimise phrase grounding performance. We note that more elaborate methods might be devised, however we leave this for future work. The red block in Fig. 1 shows the process for generating the heatmap \mathbf{h} . Furthermore, as detailed in section IV-E, results can be refined by applying additional post-processing techniques on

the generated heatmap \mathbf{h} that do not involve any learnable parameters or any form of supervision, thus not violating the zero-shot scenario.

IV. EXPERIMENTAL RESULTS

A. LDM Pre-training Setup

First, we briefly discuss the LDM pre-training stage. Here, we use an open-source implementation of the LDM along with a provided checkpoint; thus, *we do not train the LDM ourselves*. For our experiments, we use the LDM architecture as defined in [18]. The model is pre-trained on MIMIC-CXR [19], a large-scale dataset of chest radiographs accompanied by free-text reports. The training set consists of 368,960 chest X-ray images, whereas the text prompt for each image is a randomly sampled sentence from the corresponding radiology report, from either the *Impressions* or *Findings* section. Note that the pre-trained weights, as well as the configuration files with all training-related details, are publicly available in the MONAI Generative framework [20].

B. Phrase Grounding Setup

The phrase grounding task is performed with the following setup: The sampled input image is first transformed into a fixed spatial dimension of 512×512 . For the diffusion process, we set the scheduler’s total timesteps to $T=300$. In terms of text processing, we use the standard CLIP text encoder with frozen weights. Prior to encoding, the input prompt is tokenized and then either padded or truncated to match the maximum sequence length ($S=77$ tokens). Since the CLIP text encoder is not trained on radiology reports, domain-specific terms such as “atelectasis” may be out-of-vocabulary (OOV). The CLIP tokenizer handles any unknown OOV token by splitting it into multiple known sub-tokens.

The size of the gathered attention maps is $\mathbb{R}^{S \times B \times B \times L \times T}$, where $L=11$ is the total number of cross-attention layers in the U-Net and B is the spatial size (either 16 or 32, depending on the layer’s level in the U-Net architecture). We first average across the token sequence dimension S , excluding any padding tokens. Then, the intensities within the spatial maps are normalized to span the range $[0, 1]$, and the maps are resized to the original input’s dimension with bi-linear interpolation. After averaging across the layer L and timestep T dimensions, following [5], [15], the resulting heatmap with resolution 512×512 is convolved with a Gaussian kernel ($\sigma=2.5$).

To further optimise performance, we experiment with the choice of layers and timesteps, as well as with post-processing techniques to enhance the resulting heatmap’s quality. Our best-performing setup is reported in Subsection IV-E, and our choices are justified via ablations found in Subsection IV-I.

C. Evaluation Dataset

We evaluate our proposed system on the MS-CXR benchmark [5] which consists of 1,153 image-sentence pairs with ground truth bounding boxes indicating the pathology. Note that this dataset is extracted from the official MIMIC-CXR

test set. We further pre-process the dataset by merging entries corresponding to the same patient and the same sentence, i.e., an image might have more than one ground truth bounding box as reference for a given text prompt, where the pathology appears in multiple locations. We made the choice to compute metrics on a per-image basis (and not per bounding box) as this matched the performance reported by [5], [15].

D. Baselines

We compare our proposed method to 4 state-of-the-art baselines trained in a discriminative manner, using either fully supervised or self-supervised learning. Fully supervised networks (*MedRPG* [12], *OmniFM-DR* [13]) are trained to correctly predict the ground truth bounding box, whereas the self-supervised networks (*BioViL* [5], *BioViL-T* [15]) are trained to maximize the cosine similarity between visual and textual features without any further ground truth annotations in a self-supervised manner. We evaluate our system against these 4 methods only since they were shown to outperform previous approaches; in fact, *BioViL-T* [15], a discriminative self-supervised model, sets the current state-of-the-art on phrase grounding. For all baseline methods considered in this work, we use the publicly available pre-trained model checkpoints provided by the respective authors.

To the best of our knowledge, a generative baseline does not yet exist for the downstream task of medical phrase grounding. Note that, at the time of writing, the concurrent work [16] has not yet released weights for their own version of the LDM.

E. Our Method

We first report the hyperparameter choices leading to our best performing setup. Inspired by a prior work that performs semantic segmentation with diffusion models [4], we gather attention maps only from the *middle timesteps* and *middle cross-attention blocks*. This choice is motivated by the following two observations. During the initial timesteps of the reverse diffusion process, the reconstructed sample’s global structure has not yet been modelled properly, thus attention masks do not convey any semantic meaning; on the contrary, towards the final timesteps, fine-grained details are added to the generated sample which, according to [4], hurt segmentation performance. Therefore, using the middle timesteps strikes a balance. Correspondingly, earlier U-Net blocks contain more information about small objects in the image, while deeper blocks are more informative for larger objects. This, in turn, means that in the former case the generated heatmap would highly activate over the entire image area, whereas in the latter case we would get high activations on large anatomical structures. Therefore, focusing on middle layers strikes a balance between these two extreme cases.

Similarly, we find that optimal results are achieved when attention maps are collected from $L=4$ layers (i.e., from the 3rd, 4th, 6th and 7th cross-attention blocks), which automatically sets their spatial size to $B=16$, and also from 60 different timesteps (i.e., from timestep 120 to 180) out of $T=300$ steps in total. Note, however, that we did not perform an exhaustive search to find the optimal combination of selected

layers and timesteps; in fact, it is possible that different settings per pathology might lead to better overall performance. We leave this for future work.

Furthermore, based on our empirical observation that the resulting heatmap activates widely over the entire input area, we apply *binary-Otsu thresholding* [21] as a post-processing step to separate the more strongly activating foreground from more weakly activating background. The output binary mask is then applied to the heatmap to suppress weak signals while leaving the foreground activations unaffected.

F. Metrics

Given a predicted heatmap H (with values in the $[0, 1]$ range) and ground truth binary segmentation mask M_{GT} which has ones within each bounding box area and zero otherwise, phrase grounding performance is measured via the following evaluation metrics:

1) *Mean Intersection over Union (mIoU)*: mIoU is a standard metric to evaluate segmentation performance. The predicted binary mask at threshold t is defined as $M_H = \{h \in H : h > t\}$. Then, IoU at given threshold t is calculated as

$$IoU_{@t} = \frac{|M_H \cap M_{GT}|}{|M_H \cup M_{GT}|}. \quad (2)$$

Here, following [5], we calculate mIoU as the average over 5 different thresholds $t \in [0.1, 0.2, 0.3, 0.4, 0.5]$.

2) *Area Under ROC Curve (AUC-ROC)*: The area under the receiver operating characteristic curve is another method to estimate segmentation performance on a per-pixel basis given H and M_{GT} . Here, we compute an estimate of AUC-ROC as the mean across 5 thresholds $t \in [0, 0.25, 0.5, 0.75, 1.0]$.

3) *Contrast-to-Noise Ratio (CNR)*: CNR as used in [5] is a threshold-agnostic measure that reflects the distribution of raw heatmap activations over the entire input. Let A denote the area within each bounding box, whereas \bar{A} is the rest of the heatmap, i.e., $H = A \cup \bar{A}$. Then, after calculating the mean μ and variance σ^2 of the raw heatmap scores for each area A and \bar{A} , respectively, CNR is defined as

$$CNR = \frac{\mu_A - \mu_{\bar{A}}}{\sqrt{\sigma_A^2 + \sigma_{\bar{A}}^2}}. \quad (3)$$

Note that this definition will penalize the case where $\mu_A < \mu_{\bar{A}}$. However, following [5], we also provide results for the absolute CNR evaluated as

$$|CNR| = \frac{|\mu_A - \mu_{\bar{A}}|}{\sqrt{\sigma_A^2 + \sigma_{\bar{A}}^2}}. \quad (4)$$

G. Evaluation Protocol

To ensure a fair comparison across all approaches, we adopt the following protocol:

- All metrics are computed on the original image dimensions. Therefore, for heatmap-based methods such as [5], [15], and our own method, we also perform nearest neighbor interpolation with appropriate zero padding to match the original image resolution. Note that each of those methods initially generates a fixed size heatmap

which matches the respective input size: for BioViL [5], the resolution is 480×480 , for BioViL-T [15] it is equal to 448×448 , while our LDM-based approach outputs a 512×512 heatmap per image. For methods [12], [13] that directly predict bounding box coordinates, those are simply resized based on the width and height of the original image.

- Since heatmaps generated with *BioViL* [5] and *BioViL-T* [15] methods are on $[-1, 1]$ range (due to cosine similarity), whereas our method yields heatmaps in the $[0, 1]$ range, we set all negative values for the aforementioned baselines [5], [15] to 0.
- Both *MedRPG* [12] and *OmniFM-DR* [13] are Transformer-based models that directly predict bounding box coordinates. Thus, we evaluate those two methods only in terms of mIoU.
- *MedRPG* [12] does not support the case where more than one bounding box exists per image. Therefore, for those images, we evaluate it on each bounding box separately and only keep the maximum value of mIoU reported for each image.

H. Results and Discussion

In this section we report results using the 4 aforementioned metrics (mIoU, AUC-ROC, $|CNR|$ and CNR), and also further discuss implications. In Subsection IV-I we illustrate strengths in our chosen approach via a separate ablation study.

Overall phrase grounding results on the MS-CXR database are reported in Table I. Note that error bars are not included in our analysis since we run all models on evaluation mode, meaning that results are deterministic.

We now provide an interpretation of the results shown in Table I. More specifically, we draw the following conclusions:

First, our proposed method outperforms both supervised baselines *MedRPG* [12] and *OmniFM-DR* [13] by a large margin. This is also the case for self-supervised baselines [5], [15] that are trained on image-text pairs. This observation suggests that free-text reports provide a rich source of information that can be used as an alternative to ground truth bounding box annotations.

Second, our method is competitive with both BioViL variants [5], [15] for most pathologies on the MS-CXR dataset. In fact, our pipeline based on the LDM sets a new state-of-the-art in terms of both mIoU (0.7 % relative improvement to BioViL-T [15]) and AUC-ROC (0.1 % relative increase to BioViL-T [15]) metrics averaged across all classes.

Moreover, given both definitions of the CNR metric presented in Eqs. (3) and (4), respectively, our method remains fairly robust between the two for most pathology classes. More specifically, our approach yields the lowest difference between $|CNR|$ and CNR for 7 out of 8 classes. Concretely, this highlights that $|CNR|$, which is reported in [5], [15], overestimates performance, thus making it less reliable.

We also observe that every method performs poorly on the *Pneumothorax* class (our approach leads to a negative CNR value). We note that pneumothorax causes a dark air space (i.e., a region with low intensity pixels) in the position of

TABLE I: Phrase grounding results on MS-CXR dataset. Results are reported across the 8 pathologies of interest and also averaged (Avg). Both |CNR| and CNR metrics are unbounded, i.e., in $(-\infty, \infty)$ range. mIoU and AUC-ROC are reported in (%). Higher is better for all metrics (\uparrow). Note that, due to implementation details, only mIoU can be computed for methods [12] and [13]. Best metrics are highlighted with **bold**. Second best metrics are underlined.

Method	Metric	Pneumonia	Pneumothorax	Consolidation	Atelectasis	Edema	Cardiomegaly	Lung Opacity	Pleural Eff.	Avg
BioViL [5]	CNR	<u>1.56</u>	<u>0.78</u>	1.79	<u>1.37</u>	0.85	0.81	<u>1.24</u>	<u>1.38</u>	<u>1.22</u>
	CNR	1.49	<u>0.63</u>	1.73	<u>1.28</u>	0.77	0.73	<u>1.18</u>	<u>1.33</u>	<u>1.14</u>
	mIoU	<u>27.3</u>	<u>10.2</u>	31.8	24.1	<u>21.3</u>	22.0	15.0	20.4	21.5
	AUC-ROC	76.5	<u>66.3</u>	<u>83.5</u>	<u>76.4</u>	<u>65.1</u>	64.5	68.9	76.6	72.2
MedRPG [12]	mIoU	11.3	5.8	6.1	12.2	5.1	16.3	6.5	11.7	9.4
OmniFM-DR [13]	mIoU	12.6	7.0	24.7	5.4	17.0	<u>30.9</u>	15.4	5.1	14.8
BioViL-T [15]	CNR	1.70	1.01	1.79	1.47	<u>0.84</u>	1.06	1.59	1.55	1.38
	CNR	1.66	0.91	1.74	1.45	0.77	1.05	1.54	1.53	1.33
	mIoU	29.0	12.6	<u>30.2</u>	<u>24.7</u>	19.0	23.5	17.5	18.6	<u>21.9</u>
	AUC-ROC	80.1	70.1	83.9	<u>76.4</u>	63.0	<u>66.1</u>	<u>76.3</u>	73.8	<u>73.7</u>
Ours	CNR	1.01	0.46	1.17	1.05	0.75	<u>0.91</u>	1.12	0.88	0.92
	CNR	1.01	-0.07	1.14	1.04	0.70	<u>0.90</u>	1.08	0.86	0.83
	mIoU	23.7	5.3	24.5	24.8	30.4	37.1	<u>16.6</u>	<u>19.2</u>	22.6
	AUC-ROC	<u>78.7</u>	49.7	80.9	78.8	72.2	75.2	79.4	<u>75.2</u>	73.8

the collapsed lung, as opposed to the other pathologies which manifest as “bright” regions. These dark regions may be more difficult to differentiate from normal lung.

I. Ablation Study

In Table II we provide an ablation study showing how different hyperparameters affect phrase grounding performance. To speed up these experiments, we set the total number of timesteps to $T = 100$ (yet the empirical observations are expected to be similar for larger T as well). Starting from the initial setup of collecting all attention maps across all timesteps ($L = 11, T = 100$), we gradually focus only on middle cross-attention blocks ($L = 6$) and middle timesteps ($T = 20$). Note that, although we got the exact same results for $T = 40$, we chose $T = 20$ since it speeds up inference. We see that the choice of middle timesteps ($L=11, T=20$) has a positive impact on both metrics. Furthermore, although the choice of middle cross-attention blocks ($L=6, T=100$) does not provide significant improvements on its own, we observe that the combination thereof ($L=6, T=20$) yields a substantial boost in performance compared to the initial setup ($L=11, T=100$). We also show the effect of post-processing the heatmap with binary Otsu thresholding. In fact, although we notice a slight decrease in CNR, mIoU is increased by 3.5%. Note also how different pathology classes might benefit from different setups, meaning that there is room for improvement.

J. Qualitative Analysis

Fig. 3 depicts examples of generated heatmaps for BioViL-T [15] and our proposed pipeline for randomly sampled image-text pairs from the MS-CXR dataset. We observe that BioViL-T provides more densely localized results compared to our method which activates on larger input areas. However, unlike BioViL-T, our method does not miss an area of interest (cf. sub-figures 3a and 3e for pathology labels *Pneumonia* and *Edema*, respectively). We note that our LDM-based method could also be focusing on less relevant anatomical regions in

some cases (cf. the right column for sub-figures 3b, 3d, 3g, respectively) that, however, can be categorized as easy false positives.

V. CONCLUSION

In this work we have presented a novel approach for performing phrase grounding with a pre-trained Latent Diffusion Model. In fact, we draw on the parts of the model that integrate visual and textual features, namely the cross-attention blocks. These blocks, as evidenced by our results, provide a rich source of information that can be readily used to solve downstream tasks. Our proposed method does not alter the backbone generative model in any way, thus operating on a zero-shot setting. We believe that further improvements on the generative aspect of the LDM, i.e., forcing the model to rely less on spurious features during reconstruction (e.g. by generating appropriate synthetic data to counteract biases [22]), will also bring a positive effect on the model’s downstream performance. In terms of this work’s broader impact, our proposed framework might be used to automatically link reports to the relevant image locations, allowing fast inclusion of key images and easy navigation when reviewing a previous scan. We might also extend to the task of diagnosis by creating text prompts such as “Where is {pathology_label}?”, to achieve an off-the-shelf detector that provides automated diagnosis (beyond the scope of this paper).

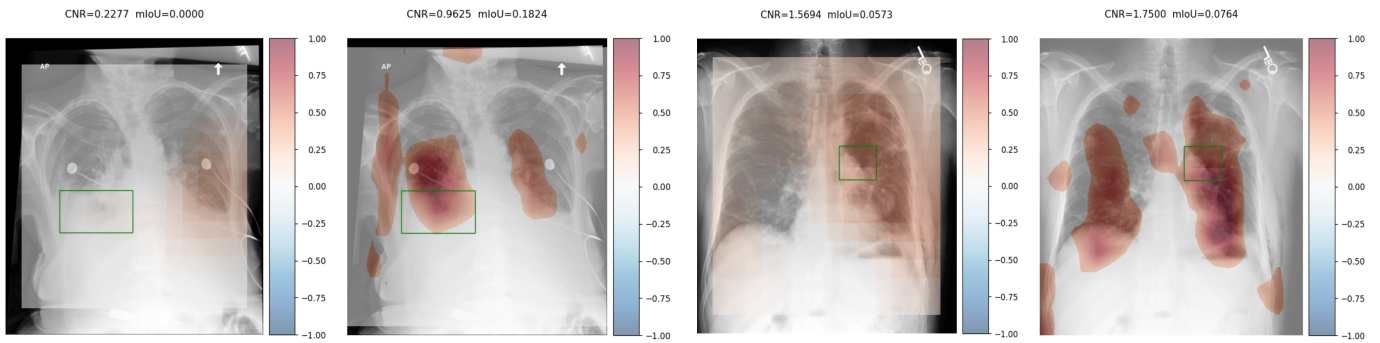
REFERENCES

- [1] R. Bommasani, D. A. Hudson, E. Adeli, *et al.*, “On the opportunities and risks of foundation models,” *arXiv preprint arXiv:2108.07258*, 2021.
- [2] A. C. Li, M. Prabhudesai, S. Duggal, E. Brown, and D. Pathak, “Your diffusion model is secretly a zero-shot classifier,” *arXiv preprint arXiv:2303.16203*, 2023.
- [3] K. Clark and P. Jaini, “Text-to-image diffusion models are zero shot classifiers,” *Advances in Neural Information Processing Systems*, vol. 36, 2024.

TABLE II: Ablation study on the choice of layers L and timesteps T , as well as the effect of post-processing on the resulting heatmap. Note that: the total number of timesteps is fixed here to $T_{total} = 100$, while $T = 20$ refers to the $[40, 60]$ range of steps. CNR metric is unbounded, mIoU is in (%). Best metrics are highlighted with **bold**.

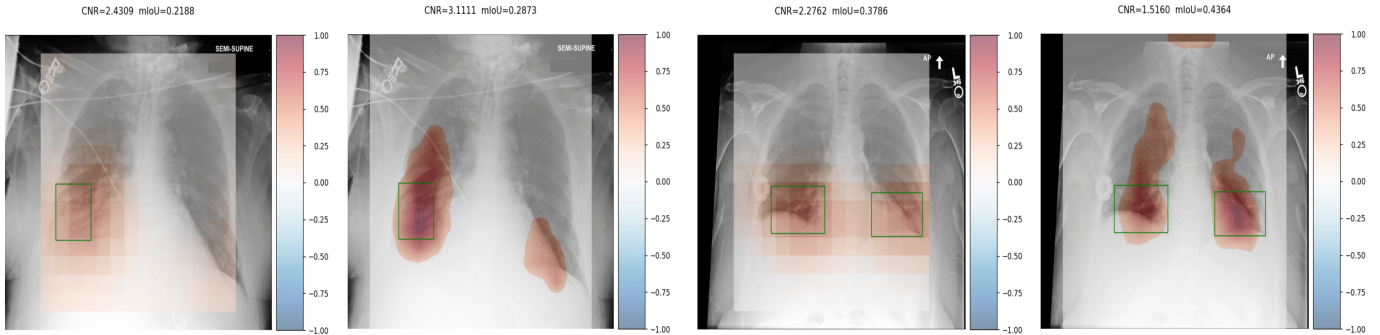
Setup	Metric	Pneumonia	Pneumothorax	Consolidation	Atelectasis	Edema	Cardiomegaly	Lung Opacity	Pleural Eff.	Avg
L=11, T=100	CNR	0.86	-0.17	0.89	0.96	0.55	0.52	0.88	0.90	0.67
	mIoU	14.7	5.4	16.1	16.1	25.0	22.8	10.6	13.6	15.5
L=11, T=20	CNR	0.87	-0.16	0.91	0.94	0.63	0.60	0.89	0.90	0.70
	mIoU	16.0	5.3	17.2	17.0	25.3	24.3	11.6	14.1	16.3
L=6, T=100	CNR	0.86	-0.17	0.89	0.97	0.56	0.52	0.89	0.90	0.68
	mIoU	14.8	5.4	16.2	16.2	25.0	22.9	10.7	13.7	15.6
L=6, T=20	CNR	0.90	-0.09	0.99	1.01	0.61	0.77	0.98	0.90	0.76
	mIoU	15.6	5.5	17.1	16.9	26.2	26.7	11.3	14.1	16.7
L=6, T=20, Otsu	CNR	0.87	-0.15	0.98	0.98	0.59	0.80	0.94	0.88	0.74
	mIoU	20.3	5.1	21.2	22.1	28.2	33.0	14.1	18.1	20.2

- [4] D. Baranchuk, I. Rubachev, A. Voynov, V. Khulkov, and A. Babenko, "Label-efficient semantic segmentation with diffusion models," *arXiv preprint arXiv:2112.03126*, 2021.
- [5] B. Boecking, N. Usuyama, S. Bannur, *et al.*, "Making the most of text semantics to improve biomedical vision-language processing," in *European conference on computer vision*, Springer, 2022, pp. 1–21.
- [6] W. Zhao, Y. Rao, Z. Liu, B. Liu, J. Zhou, and J. Lu, "Unleashing text-to-image diffusion models for visual perception," *arXiv preprint arXiv:2303.02153*, 2023.
- [7] J. Lu, D. Batra, D. Parikh, and S. Lee, "Vilbert: Pre-training task-agnostic visiolinguistic representations for vision-and-language tasks," *Advances in neural information processing systems*, vol. 32, 2019.
- [8] A. Kamath, M. Singh, Y. LeCun, G. Synnaeve, I. Misra, and N. Carion, "Mdetr-modulated detection for end-to-end multi-modal understanding," in *Proceedings of the IEEE/CVF International Conference on Computer Vision*, 2021, pp. 1780–1790.
- [9] L. H. Li, P. Zhang, H. Zhang, *et al.*, "Grounded language-image pre-training," in *Proceedings of the IEEE/CVF Conference on Computer Vision and Pattern Recognition*, 2022, pp. 10965–10975.
- [10] S. Chen and B. Li, "Language-guided diffusion model for visual grounding," *arXiv preprint arXiv:2308.09599*, 2023.
- [11] R. Bhalodia, A. Hatamizadeh, L. Tam, *et al.*, "Improving pneumonia localization via cross-attention on medical images and reports," in *Medical Image Computing and Computer Assisted Intervention–MICCAI 2021: 24th International Conference, Strasbourg, France, September 27–October 1, 2021, Proceedings, Part II 24*, Springer, 2021, pp. 571–581.
- [12] Z. Chen, Y. Zhou, A. Tran, *et al.*, "Medical phrase grounding with region-phrase context contrastive alignment," in *International Conference on Medical Image Computing and Computer-Assisted Intervention*, Springer, 2023, pp. 371–381.
- [13] L. Xu, Z. Ni, X. Liu, X. Wang, H. Li, and S. Zhang, "Learning a multi-task transformer via unified and customized instruction tuning for chest radiograph interpretation," *arXiv preprint arXiv:2311.01092*, 2023.
- [14] G. Dawidowicz, E. Hirsch, and A. Tal, "Limitr: Leveraging local information for medical image-text representation," *arXiv preprint arXiv:2303.11755*, 2023.
- [15] S. Bannur, S. Hyland, Q. Liu, *et al.*, "Learning to exploit temporal structure for biomedical vision-language processing," in *Proceedings of the IEEE/CVF Conference on Computer Vision and Pattern Recognition*, 2023, pp. 15016–15027.
- [16] M. Dombrowski, H. Reynaud, J. P. Müller, M. Baugh, and B. Kainz, *Trade-offs in fine-tuned diffusion models between accuracy and interpretability*, 2023. arXiv: 2303.17908 [cs.CV].
- [17] R. Rombach, A. Blattmann, D. Lorenz, P. Esser, and B. Ommer, "High-resolution image synthesis with latent diffusion models," in *Proceedings of the IEEE/CVF conference on computer vision and pattern recognition*, 2022, pp. 10684–10695.
- [18] W. H. Pinaya, P.-D. Tudosiu, J. Dafflon, *et al.*, "Brain imaging generation with latent diffusion models," in *MICCAI Workshop on Deep Generative Models*, Springer, 2022, pp. 117–126.
- [19] A. E. Johnson, T. J. Pollard, N. R. Greenbaum, *et al.*, "Mimic-cxr-jpg, a large publicly available database of labeled chest radiographs," *arXiv preprint arXiv:1901.07042*, 2019.
- [20] W. H. Pinaya, M. S. Graham, E. Kerfoot, *et al.*, "Generative ai for medical imaging: Extending the monai framework," *arXiv preprint arXiv:2307.15208*, 2023.
- [21] P.-S. Liao, T.-S. Chen, P.-C. Chung, *et al.*, "A fast algorithm for multilevel thresholding," *J. Inf. Sci. Eng.*, vol. 17, no. 5, pp. 713–727, 2001.
- [22] F. Pérez-García, S. Bond-Taylor, P. P. Sanchez, *et al.*, "Radedit: Stress-testing biomedical vision models via diffusion image editing," *arXiv preprint arXiv:2312.12865*, 2023.



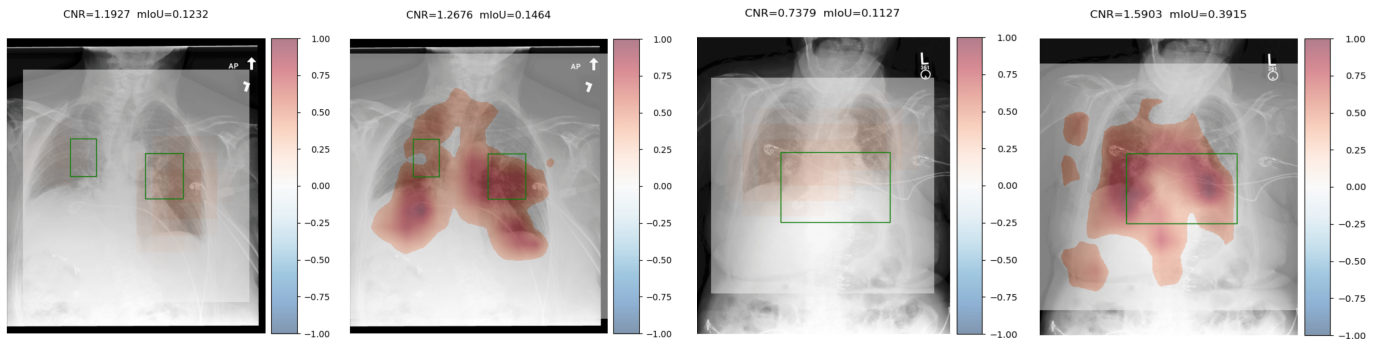
(a) Basal consolidations could represent atelectasis versus aspiration/pneumonia

(b) fluid level posteriorly, which represents a loculated hydropneumothorax



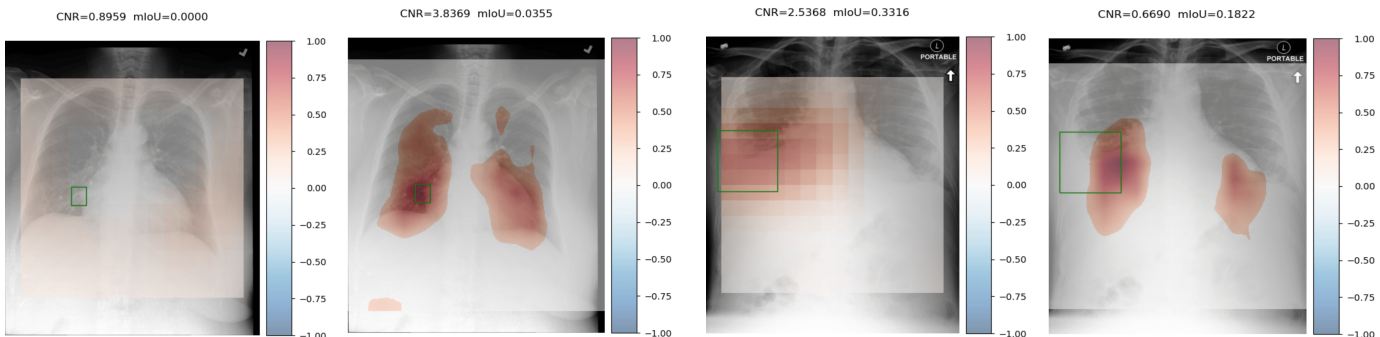
(c) patchy consolidation of the right lung base

(d) bibasilar atelectasis noted



(e) peribronchial cuffing consistent with mild pulmonary edema

(f) enlarged cardiac silhouette (class: **Cardiomegaly**)



(g) Minimal residual right middle lobe opacity, otherwise clear lungs

(h) Moderate right pleural fluid remains (class: **Pleural Effusion**)

Fig. 3: Qualitative results for the phrase grounding task. For each image-text pair, we overlay the generated heatmaps from *BioViL-T* [5] (left column of each pair) and our own method (right column of each pair) on top of the original images. The grey shaded area in each figure shows the center crop that is used as input for each method. We provide the accompanying text prompt for each image as a caption in each sub-figure. Ground truth classes are highlighted in **bold**. For completeness, in cases where the ground truth class is not explicitly mentioned in the prompt, we refer to it in parentheses. Ground-truth bounding boxes are depicted in green. The samples are randomly drawn such that each pathology class is represented once. For each image, we also provide the reported $|CNR|$ and mIoU metrics per method (shown on top of each plot). Best viewed in colour.